Electronic Supplementary Material (ESI) for Energy & Environmental Science

Supplemental Information for Photoelectrochemistry of Core–Shell Tandem Junction n-p$^+$-Si/n-WO_3 Microwire Array Photoelectrodes

[★,○]*Matthew R. Shaner*, [★,○]*Katherine T. Fountaine*, [★]*Shane A. Ardo*, [★]*Robert H. Coridan*, [#,○]*Harry A. Atwater**, [★,○]*Nathan S. Lewis**

[★]Division of Chemistry and Chemical Engineering, M/C 127-72

[#]Thomas J. Watson, Sr. Laboratories of Applied Physics, M/C 180-32

[○]Joint Center for Artificial Photosynthesis, M/C 132-80

1200 E. California Blvd.

California Institute of Technology

Pasadena, CA 91125, USA

Table S1: Refractive index source for light absorption modeling

Material	**n,k source**
Si	Aspnes[1]
WO_3	Ellipsometry (Figure S1)
ITO	Ref. [2]
SiO_2	Palik[3]

Table S2: Geometric parameters for the Si/WO_3 microwire structure in Figure 1b used for the optical modeling

Si Microwire diameter (d)	1.8 μm
Si Microwire height (h)	80 μm
Si Microwire pitch (p)	7 μm
Si substrate thickness (t_{Si})	Infinite
SiO_2 boot height (h_{boot})	20 μm
SiO_2 boot thickness (t_{boot})	100 nm
SiO_2 base thickness (t_{base})	500 nm
ITO thickness (t_{ITO})	50 nm
WO_3 coating thickness (t_{WO3})	500 nm
WO_3 top thickness (t_{WO3top})	2.3 μm

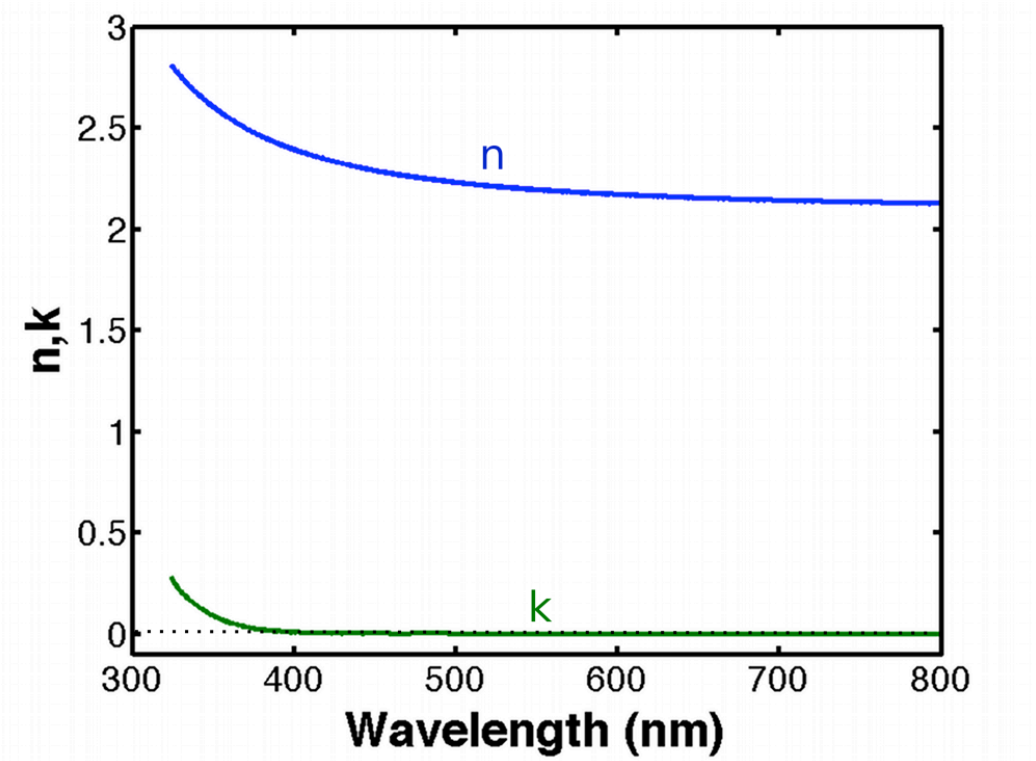

Figure S1: Refractive index data for WO_3. The real component of the refractive index, n, was obtained by fitting ellipsometry data and extrapolating above the bandgap with a Lorentzian function. Given the *n* obtained by ellipsometry, an adapted form of a multilayer material transfer matrix program was used to fit integrating sphere transmission data to extract the imaginary component of the refractive index, *k*.

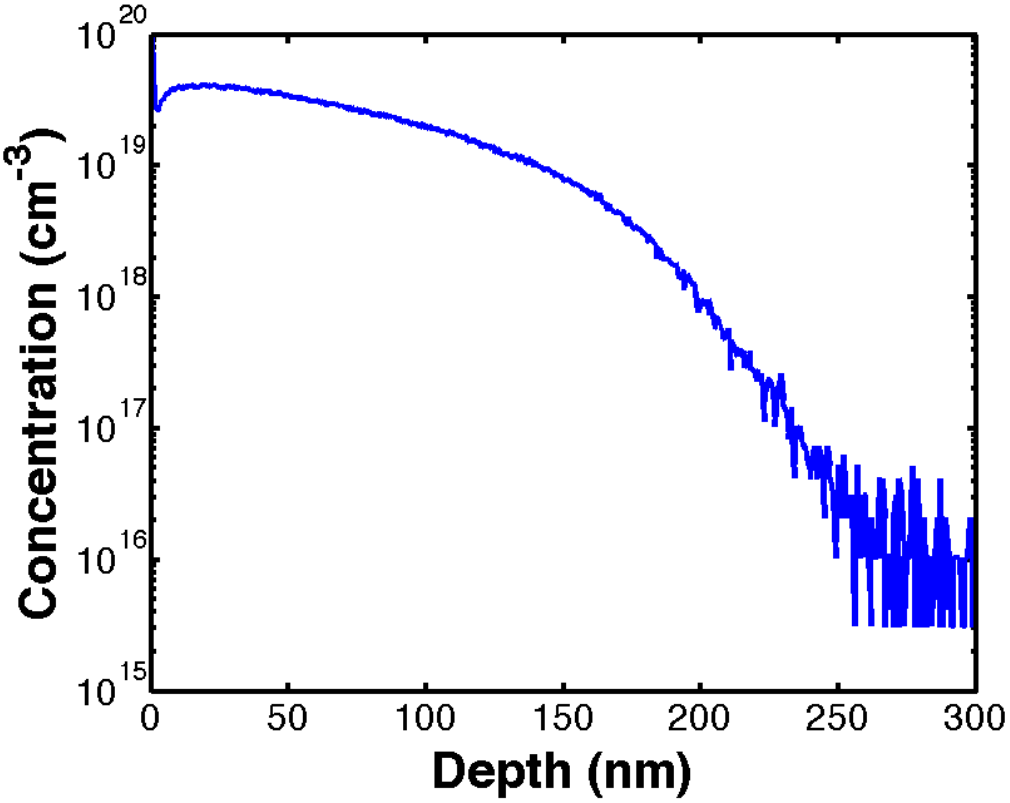

Figure S2: Concentration profile of boron in an n-Si planar wafer after BCl_3 drive in, from a secondary ion mass spectrometry (SIMS) measurement (see experimental section). This shows an emitter thickness of ~250 nm.

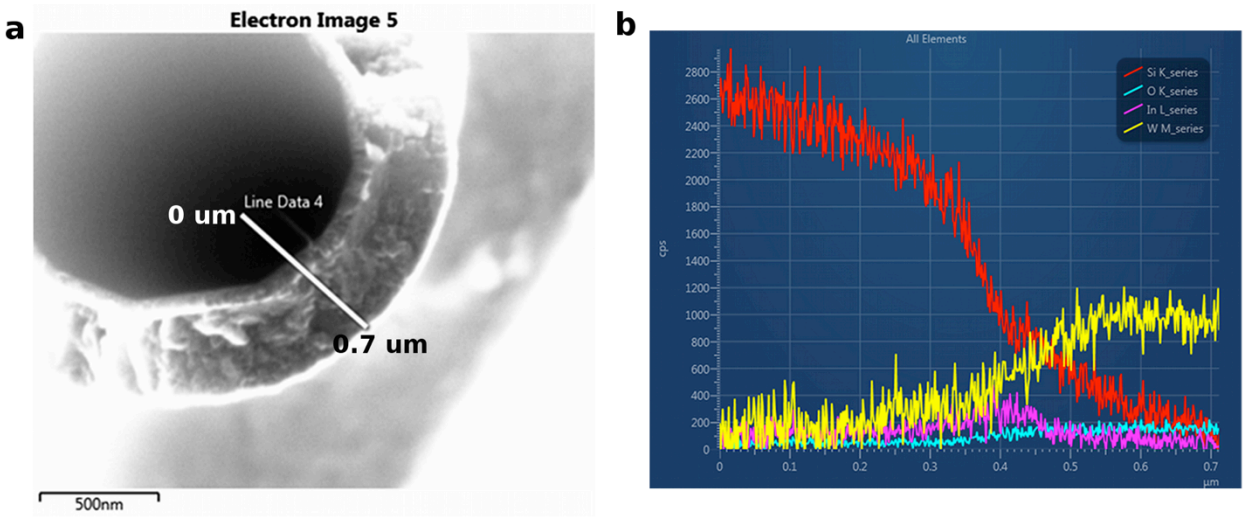

Figure S 3: a) SEM image captured by the EDX instrument of a tandem microwire cross section. The line scan performed is overlaid on this image with the beginning and end indicated. b) Line scan data as reported by the Oxford Aztec software. It shows a clear transition from a Si rich area (<0.35 µm) to an indium rich area (0.35 µm-0.45 µm) to a W and O rich area (>0.45 µm). This further verifies the presence of the layered structure as described in the main text.

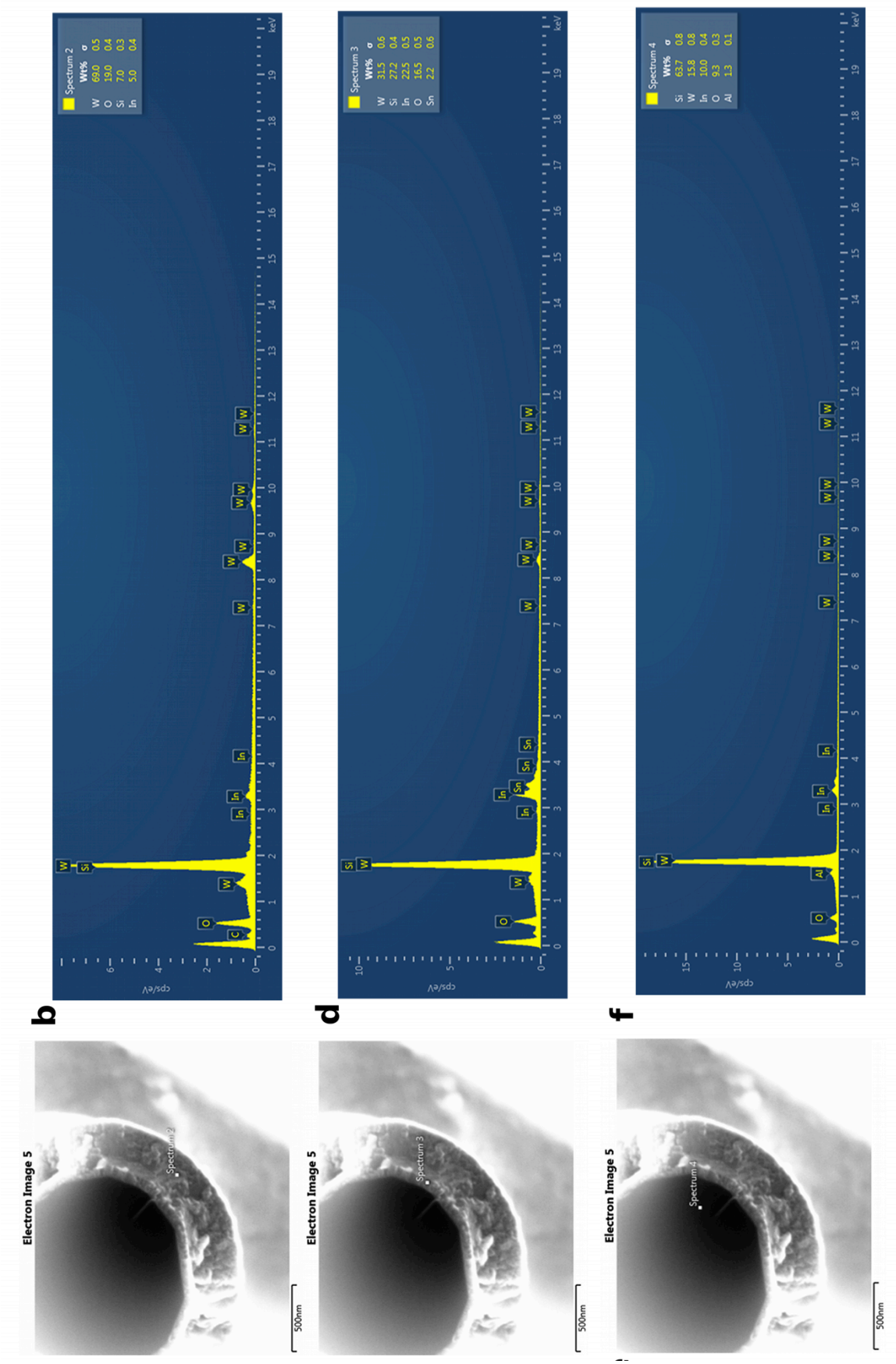

Figure S 4: (a), (c), (e) SEM images captured by the EDX software that indicated the point where data was taken at. (b), (d,) (f) Corresponding EDX data the points depicted in (a), (c), (e.) These data also confirm the layered structure described in the text.

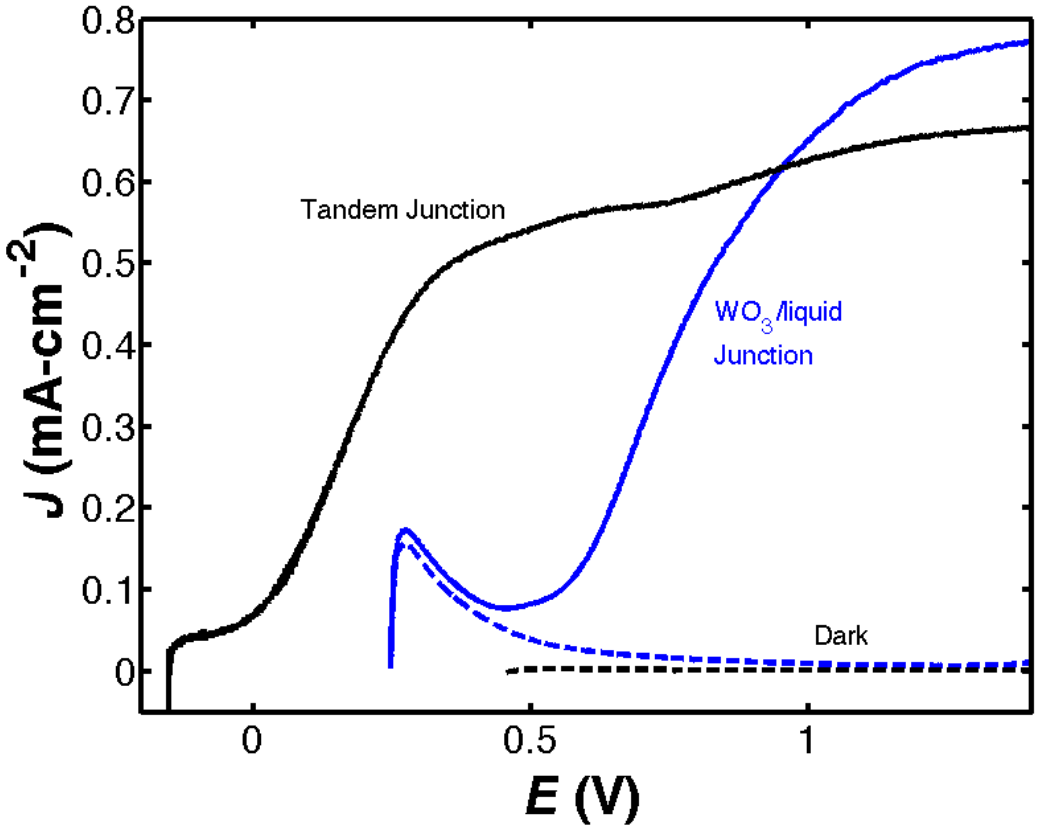

Figure S 5: Planar single (WO_3/liquid) and tandem (n-Si/p^+-Si/ITO/WO_3/liquid) junction current density vs. potential behavior in 1.0 M H_2SO_4 under one Sun illumination (AM 1.5G).

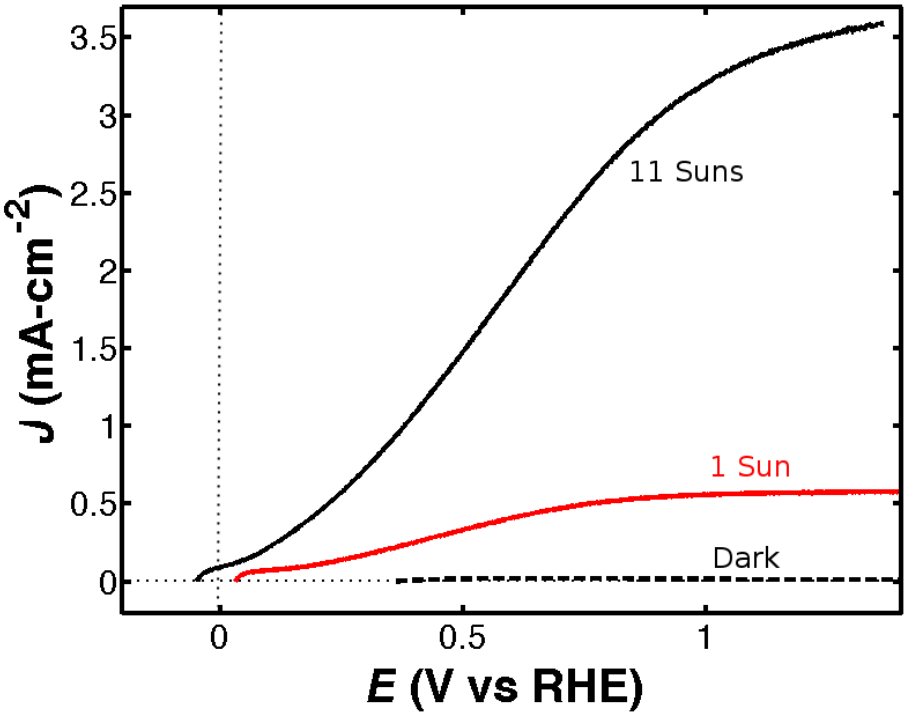

Figure S6: Effect of concentrated illumination on tandem-junction WO_3/Si microwire photoelectrochemical performance in 1.0 M H_2SO_4. Data shown are for the potential sweep at 20 mV-s^{-1}.

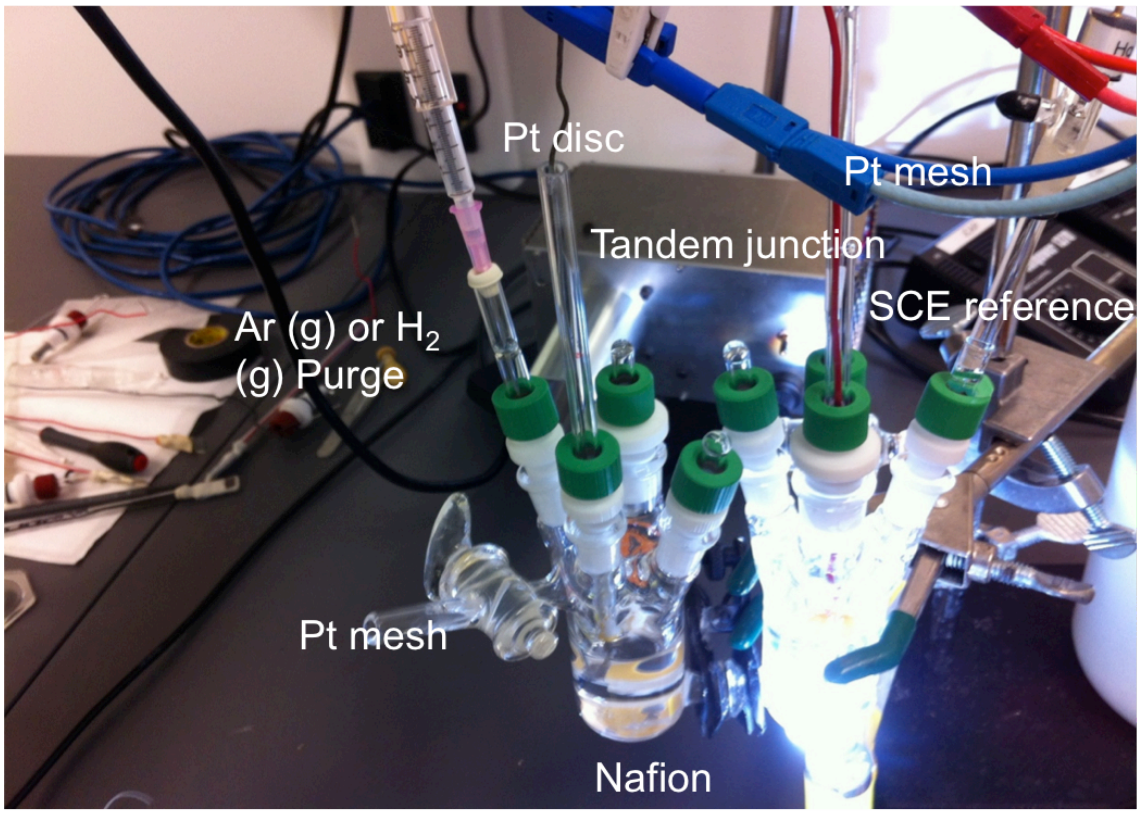

Figure S7: Two-cell, three- or two-electrode evaluation set-up with the cathode compartment on the left and anode compartment on the right. The cathode compartment is sealed, continually purged with an Ar or H_2 gas stream, and contains ports for the Pt disc electrode and Pt mesh counter electrode. The anode compartment contains the tandem junction electrode illuminated through a quartz window, an SCE reference electrode, and a Pt mesh counter electrode. The cells are separated by a Nafion membrane sandwiched between flanges on the sides of the cells and held together with a clamp.

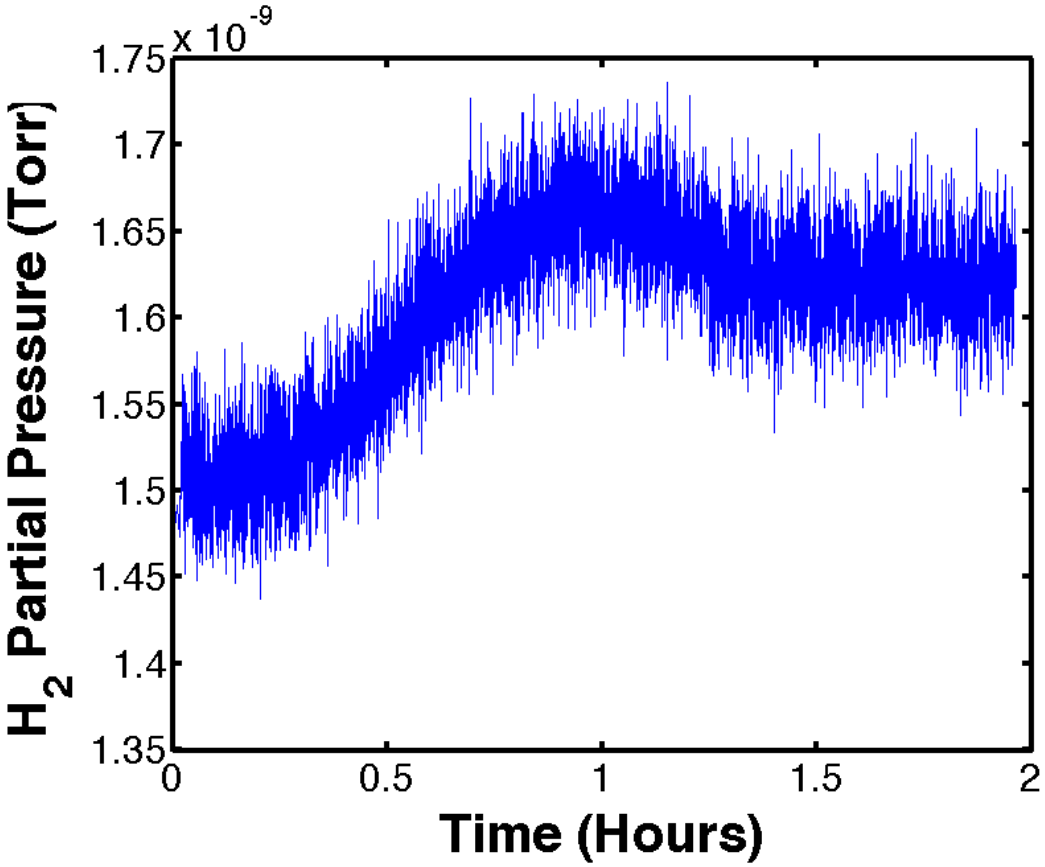

Figure S8: Mass spectrometry data for H_2 detection at a Pt disc electrode.

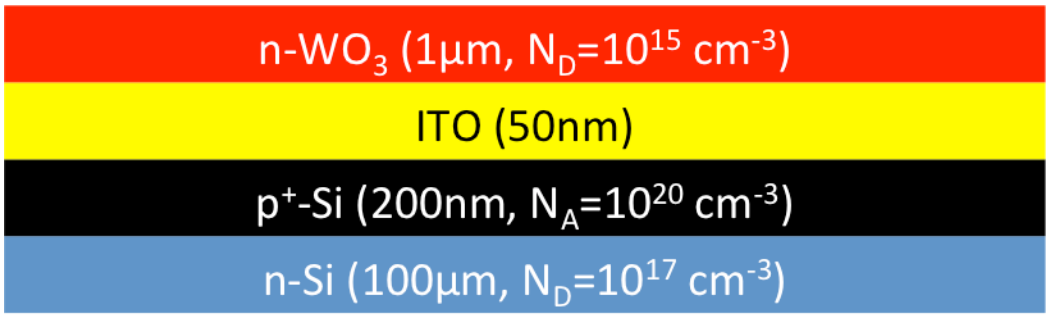

Figure S9: Structure used to model the absorption in the 1D optoelectronic model. Each junction (n-p^+-Si and n-WO_3/liquid) was modeled individually.

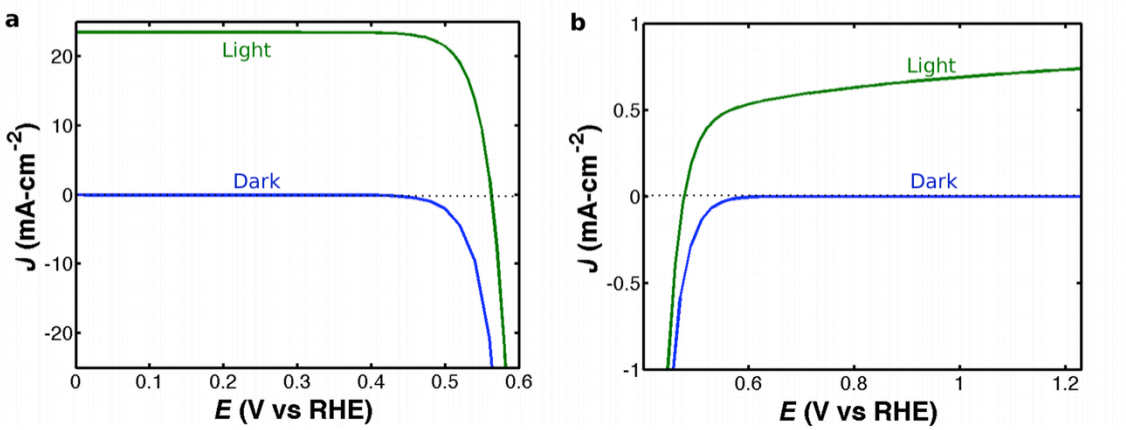

Figure S10: Modeled light (1 sun) and dark *J*–*E* behaviour for (a) an n-p$^+$-Si homojunction and (b) an n-WO_3/$E^{o\prime}$(O_2/H_2O) liquid junction.

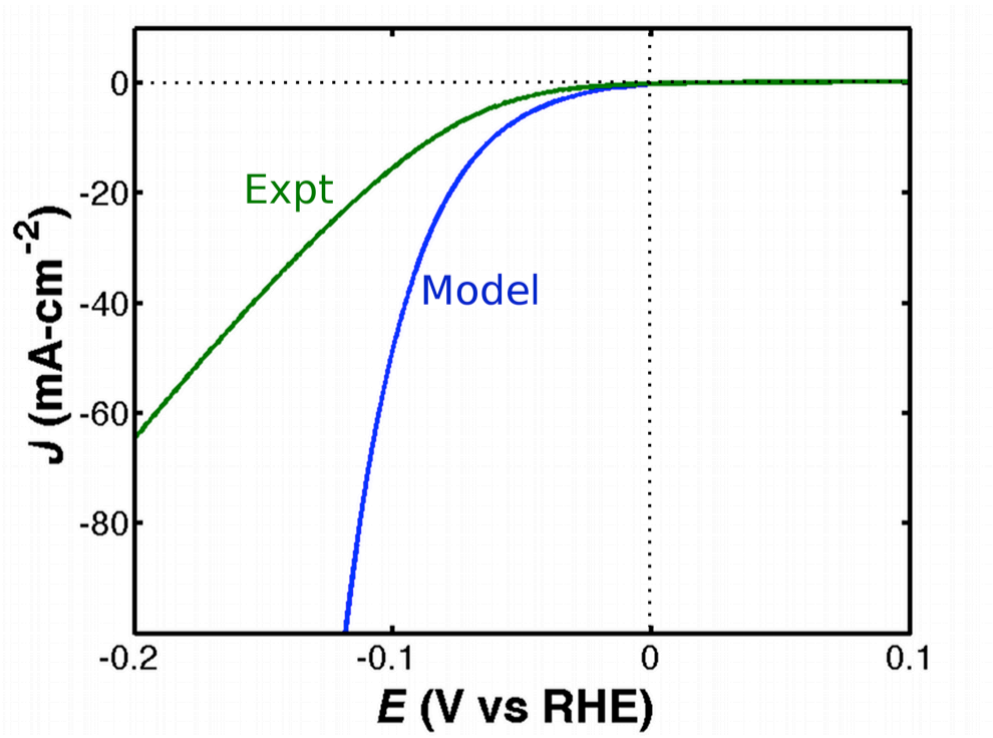

Figure S11: Experimental (green) and modeled (blue) hydrogen evolution *J-E* behaviour. The experimental data includes solution and mass transport resistances that were not included in the modeled data. Thus the modeled data represents an ideal system where solution and mass transport resistances are absent.

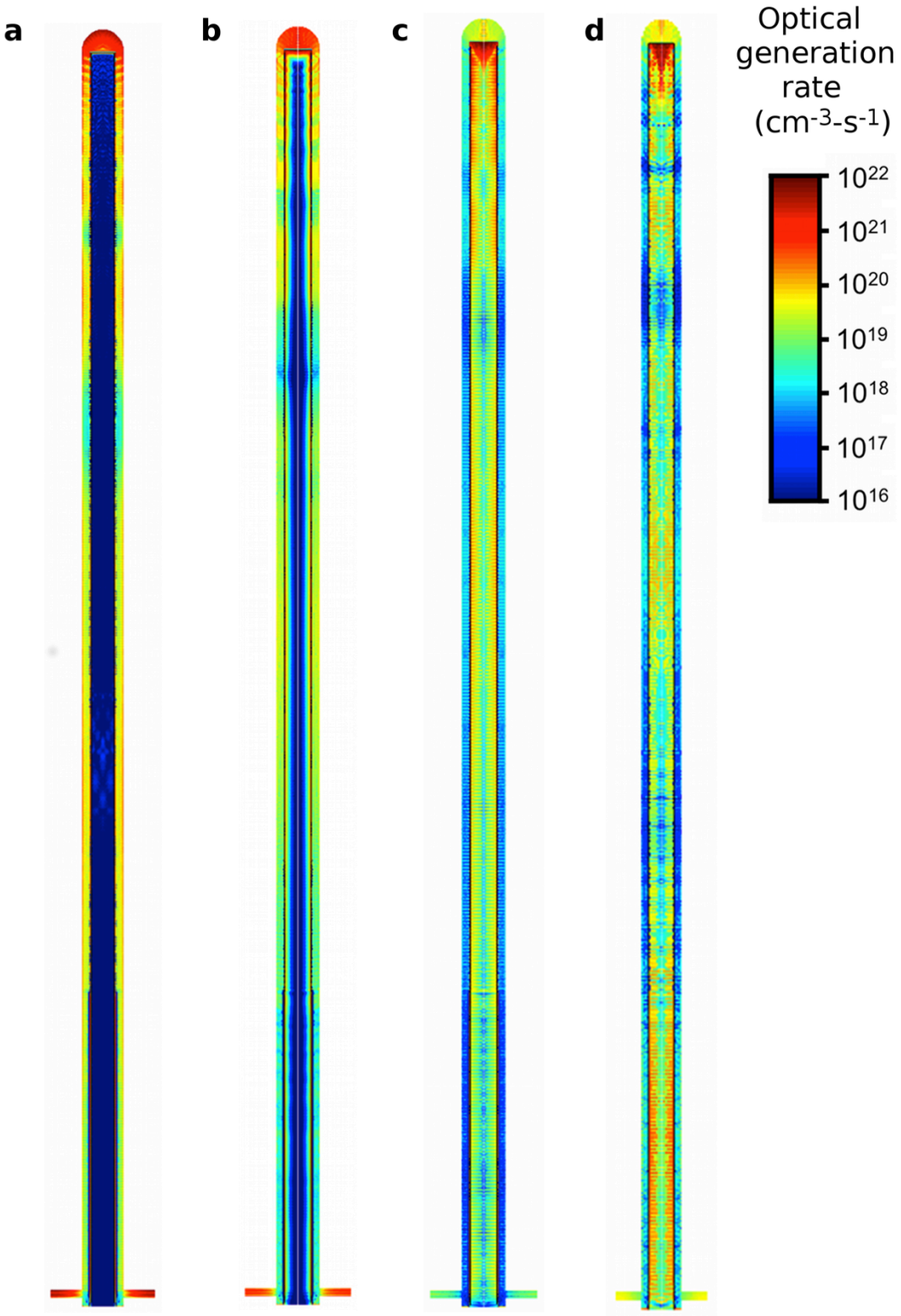

Figure S12: Carrier generation rate map for four wavelengths: (a) 350 nm, (b) 400 nm, (c) 450 nm, and (d) 500 nm.

References

(1) *D. E. Aspnes. Optical properties of Si. In Hull, editor, Properties of Crystalline Silicon, page 677. INSPEC, IEE, London UK, 1999.*

(2) *Dobrowolski, J.A.; Li, L.; Hilfiker, J.N. Applied Optics 38, 22 (1999).*

(3) *E. D. Palik. Handbook of Optical Constants of Solids. New York, Academic Press, 1997.*